ter agreement between theory and experiment. At the present level of accuracy, the present agreement indicates that the Chéveau model is adequate for the interpretation of x-ray Debye-Waller-factor data of cubic metals.

ACKNOWLEDGMENTS

The authors are thankful to the Council of Scientific and Industrial Research, New Delhi, for financial support, and to Professor Vachaspati for encouragement.

[1]A. Paskin, Acta Cryst. 10, 667 (1957).
[2]J. de Launay, J. Chem. Phys. 21, 1975 (1953); in *Solid State Physics*, edited by F. Seitz and D. Turnbull (Academic, New York, 1956), Vol. 2, p. 220.
[3]A. B. Bhatia, Phys. Rev. 97, 363 (1955); A. B. Bhatia and G. K. Horton, *ibid.* 98, 1715 (1955).
[4]P. K. Sharma and S. K. Joshi, J. Chem. Phys. 39, 2633 (1963); 40, 662 (1964).
[5]M. Lax, in *Proceedings of the International Conference on Lattice Dynamics, Copenhagen*, 1963, edited by R. F. Wallis (Pergamon, New York, 1964), p. 179.
[6]K. Krebs, Phys. Rev. 138, A143 (1965).
[7]L. Chéveau, Phys. Rev. 169, 496 (1968).
[8]P. K. Sharma and N. Singh, Phys. Rev. B 1, 4635 (1970).
[9]R. W. James, *The Optical Principles of the Diffraction of X-rays* (G. Bell and Sons, London, 1954), p. 193.
[10]M. Blackman, in *Handbuch der Physik*, edited by S. Flügge (Springer, Berlin, 1955), Vol. 7, p. 325.
[11]P. A. Flinn, G. M. McManus, and J. A. Rayne, Phys. Rev. 123, 809 (1961).
[12]E. A. Owen and R. W. Williams, Proc. Roy. Soc. (London) A188, 509 (1947).
[13]D. R. Chipman and A. Paskin, J. Appl. Phys. 30, 1992 (1959).
[14]J. Boskovits, M. Roilos, A. Theodossiou, and K. Alexopoulos, Acta Cryst. 11, 845 (1958).
[15]R. Andriessen, Physica 2, 417 (1935).
[16]J. Spreadborough and J. W. Christian, Proc. Phys. Soc. (London) 74, 609 (1959).
[17]C. W. Haworth, Phil. Mag. 5, 1229 (1960).
[18]M. Simerská, Acta Cryst. 14, 1259 (1961).
[19]I. Backhurst, Proc. Roy. Soc. (London) A102, 340 (1922).
[20]E. H. Collins, Phys. Rev. 24, 152 (1926).
[21]R. W. James, G. W. Brindley, and R. G. Wood, Proc. Roy. Soc. (London) A125, 401 (1929).
[22]D. R. Chipman, J. Appl. Phys. 31, 2012 (1960).
[23]P. A. Flinn and G. M. McManus, Phys. Rev. 132, 2458 (1963).
[24]M. Simerská, Czech. J. Phys. B12, 858 (1962).
[25]R. H. Wilson, E. F. Skelton, and J. L. Katz, Acta Cryst. 21, 635 (1966).
[26]R. H. V. M. Dawton, Proc. Phys. Soc. (London) 49, 294 (1937).
[27]V. A. Ilyina and V. K. Kristsaya, in *Problems of Metallography and Physics of Metals, IV Symposium, Moscow*, 1955, edited by B. Ya Lyubov (English translation: U.S. Atomic Energy Commission Report No. 2924, U.S. GPO, Washington, D.C., 1956).
[28]F. H. Herbstein and J. Smuts, Phil. Mag. 8, 367 (1963).
[29]P. Debrunner and R. J. Morrison, Rev. Mod. Phys. 36, 463 (1964) [as quoted in J. Baijal, Phys. Letters 13, 32 (1964)].
[30]W. Cochran, Rept. Progr. Phys. 26, 1 (1963).
[31]H. Hahn and W. Ludwig, Z. Physik 161, 404 (1961).
[32]A. A. Maradudin and P. A. Flinn, Phys. Rev. 129, 2529 (1963).
[33]R. A. Cowley, Advan. Phys. 12, 421 (1963).

PHYSICAL REVIEW B VOLUME 3, NUMBER 4 15 FEBRUARY 1971

Graphite Carrier Locations and Quantum Transport to 10 T (100 kG)

John A. Woollam
National Aeronautics and Space Administration, Cleveland, Ohio 44135
(Received 12 June 1970)

The magnetoresistance, Hall effect, thermopower, thermal resistivity, and Nernst-Ettingshausen effects are measured in magnetic fields to 10.3 T (103 kG) and at temperatures between 1.1 and 4.2 K. Samples are highly ordered pressure-annealed pyrolytic graphite. The major results are that majority-carrier electrons and holes are assigned to specific locations in the Brillouin zone; the electrons are assigned to be around the center of the zone edge (point K). The first observation of spin-split Landau levels is made. A study of distorted line shapes of thermopower quantum oscillations shows agreement with a theory by Horton. Sugihara and Ono's theory, predicting field values for Landau level crossings of the Fermi energy in graphite, is confirmed for fields below 4 T.

I. INTRODUCTION

Pressure-annealed pyrolytic graphite is a highly ordered form of carbon, [1] but is not a single crystal. The lattice for a single crystal is hexagonal. For pyrolytic samples there are individual crystallites with [0001] axes nearly parallel to each other, but [1100] axes, for example, are randomly oriented with respect to each other. Typical crystallite sizes are between 10 and 100 μ in diam. Because

of the nature of the Fermi surface of graphite, the properties of pyrolytic and natural single crystals are very similar, as shown in this and other papers.

Fermi-surface studies of natural single crystals of graphite were made by Soule, McClure, and Smith[3] in fields to 2.4 T (1 T = 10 kG) using the Shubnikov–de Haas effect. de Haas–van Alphen studies on pressure-annealed pyrolytic graphite were made by Williamson *et al.*[2] Magnetoreflection results[4] were used along with the de Haas–van Alphen effect to determine the magnitude of the parameters necessary to describe the energy-band structure derived by Slonczewski and Weiss (SW).[5]

The location of electron and hole majority carriers in the Brillouin zone was first determined from cyclotron resonance by Galt *et al.*[6] Soule later studied the effect of boron doping on the de Haas–van Alphen frequencies.[7] Boron adds positive charge and thus shifts the Fermi energy and changes the cross-sectional areas. The shifts in majority-carrier frequencies determine the location of electron and hole carriers in the Brillouin zone and thus the signs of several of the parameters in the SW[5] band theory. Soule's results agreed with the assignment by Galt *et al.* Recently, Schroeder, Dresselhaus, and Javan[8] have used magnetoreflection and reintrepreted the results of Galt *et al.* to determine the band-parameter signs; they found a conflict with the assignment deduced from majority-carrier de Haas–van Alphen frequency shifts. In this paper we use two independent methods to help resolve the conflict between magnetoreflection and doped majority-carrier de Haas–van Alphen experiments.[9] Quantum extrema in the Hall coefficient are compared with a theory by Argyres[10] and from this a direct determination of electron and hole carrier positions in the Brillouin zone is made. This then determines the signs of the band parameters. Quantum resonances in the thermopower are used as a second and independent method of determining carrier locations and band-parameter signs. Recently, other authors[11–13] have presented additional evidence agreeing with the results of this paper as well as the conclusions of Schroeder *et al.* as to the signs of the band parameters. An excellent review of the history of the assignment of carrier locations has recently been given by McClure.[14]

The electron spin resonance was studied as a function of temperature by Wagoner[15] and an effective g factor determined which is an average over all carriers in the Brillouin zone for particular magnetic field directions. We have made the first observation of spin splitting of Landau levels in graphite.[16] From these it should be possible to determine the splitting at particular points in the Brillouin zone rather than an averaged value.

In this paper the first studies of quantum thermomagnetic effects in graphite are made, as well as Shubnikov–de Haas studies in pyrolytic graphite. Temperatures range from 1.0 to 4.2 K and fields up to 10.3 T are used. Thermopower quantum oscillations have highly distorted line shapes, and these are compared with various theories. The Shubnikov–de Haas results are compared with the theories of Adams and Holstein.[17] Sugihara and Ono[18] have calculated the positions in field for Landau level crossings of the Fermi energy and show that at high fields the crossings are not predicted by strict periodicity in inverse magnetic field. Experimental and theoretical crossings are compared for each of the observed effects.

II. THEORY

A. Kinetic Equations and Transport Coefficients

The linear relations between current density $\vec{J}$, electric field $\vec{E}$, negative temperature gradient $\vec{G}$, and heat current density $\vec{w}$ may be written[19] as

$$\vec{E}^* = \overleftrightarrow{\rho}' \cdot \vec{J} + \overleftrightarrow{\epsilon}' \cdot \vec{w}^* , \tag{1}$$

adiabatic

$$\vec{G} = \overleftrightarrow{\pi}' \cdot \vec{J} + \overleftrightarrow{\gamma} \cdot \vec{w}^* , \tag{2}$$

or independently as

$$\vec{E}^* = \overleftrightarrow{\rho} \cdot \vec{J} + \overleftrightarrow{\epsilon} \cdot \vec{G} , \tag{3}$$

isothermal

$$\vec{w}^* = -\overleftrightarrow{\pi} \cdot \vec{J} + \overleftrightarrow{\lambda} \cdot \vec{G} , \tag{4}$$

where E^* is the measured electric field

$$\vec{E}^* = \vec{E} - \vec{\nabla}\mu/e , \tag{5}$$

$$\vec{w}^* = \vec{w} - \mu\vec{J}/e , \tag{6}$$

and μ is the chemical potential. From (1) and (3), when $\vec{J}$ is zero,

$$\overleftrightarrow{\epsilon}' \cdot \vec{w} = \overleftrightarrow{\epsilon} \cdot \vec{G} , \tag{7}$$

where $\overleftrightarrow{\epsilon}$ is the isothermal thermoelectric tensor and $\overleftrightarrow{\epsilon}'$ is the adiabatic thermoelectric power.

Equation (2) shows that when $\vec{J} = 0$,

$$\vec{G} = \overleftrightarrow{\gamma} \cdot \vec{w} , \tag{8}$$

so

$$\overleftrightarrow{\epsilon}' = \overleftrightarrow{\epsilon} \cdot \overleftrightarrow{\gamma} , \tag{9}$$

where $\overleftrightarrow{\gamma}$ is the thermal-resistivity tensor, and

$$\overleftrightarrow{\gamma} = \overleftrightarrow{\lambda}^{-1} , \tag{10}$$

so

$$\overleftrightarrow{\epsilon} = \overleftrightarrow{\epsilon}'\lambda , \tag{11}$$

where $\overleftrightarrow{\lambda}$ is the thermal-conductivity tensor.

In the present experiments, transport coefficients were measured as a function of magnetic field strength, temperature, and angle between the magnetic field and the [0001] ("C") axis of graphite.

The specific coefficients measured were the yy and yx components of the $\overleftrightarrow{\rho}$, $\overleftrightarrow{\epsilon}'$, and $\overleftrightarrow{\gamma}$ tensors. In addition, the following coefficients were calculated: σ_{yy} and σ_{xy} from

$$\overleftrightarrow{\sigma} \equiv \overleftrightarrow{\rho}^{-1} , \tag{12}$$

λ_{xy} and λ_{yy} from (10), and ϵ_{yy} from (11). It is important to point out that the coefficient ϵ_{yy}, known as the isothermal thermopower, is the *negative* of the "absolute thermopower" or "thermopower" S, defined by some authors, e.g., Ziman.[20] In this paper we will use S for the thermopower, not ϵ_{yy}.

B. Adams and Holstein Theory for σ_{yy}

Adams and Holstein[17] calculate the electrical conductivity σ_{yy} for the case of crossed electric and magnetic fields for both degenerate and nondegenerate solids. Pertinent to this paper is their calculation of the conductivity for degenerate systems in the limit of large magnetic fields and low temperatures. Their calculation is quantum mechanical in that a density-matrix formalism is used, and the calculation considers various types of scattering mechanisms.

At zero degrees σ_{yy} has infinite discontinuities where the Fermi energy E_F and the Landau level coincide. That is, when

$$E_F = (n+\gamma)\hbar\omega , \tag{13}$$

where n is the Landau-level quantum number, γ is a phase factor, and the cyclotron frequency ω is given by

$$\omega = eH/m^*c , \tag{14}$$

where H is the magnetic field, and m^* is the effective mass.

In this paper we compare experimental Landau level crossings of the Fermi energy with a theoretical calculation by Sugihara and Ono.[18] The experimental magnetic field values for crossings essentially depend on the fundamental concept expressed above,[17] that at zero degrees the conductivity diverges at coincidence of E_F and the Landau level. At nonzero temperatures the divergences become sharp spikes, and at higher temperatures they become oscillations in magnetic field given by

$$\sigma_{yy} \propto \sigma_{yy}^0 \left(\frac{\hbar\omega}{E_F}\right)^{1/2} \sum_M \frac{2\pi^2 MkT}{\hbar\omega} \times \left[\sinh\left(\frac{2\pi^2 MkT}{\hbar\omega}\right)\right]^{-1} \times (2\pi M)^{-1/2} \cos\left(\frac{2\pi F}{H} - \frac{\pi}{4} - \pi M\right) , \tag{15}$$

where σ_{yy}^0 is the nonoscillatory part of σ_{yy}, and F is the de Haas–van Alphen frequency, proportional to the extremal cross-sectional area of the Fermi surface perpendicular to the magnetic field. The frequency F is related to E_F and ω by $F/H = E_F/\hbar\omega$. Equation (15) shows that the conductivity oscillates periodically in $1/H$.

Adams and Holstein[17] find that ionized impurity scattering and scattering from acoustic lattice vibrations affect only the oscillation amplitudes and not shapes. In this paper a major concern is with the oscillation shapes and position in magnetic field. In graphite, at temperatures between 1 and 4 K, the dominant scattering is expected to be from ionized impurities in natural single crystals.[21] In pyrolytic samples Spain[13] has suggested that additional scattering would occur at boundaries between crystallites. It should be pointed out that even when phonon scattering is not predominant, the Landau levels can be thermally broadened, and as demonstrated in this paper, this can strongly affect the oscillation shapes and position in magnetic field.

In graphite the effective masses are so small[3] that for fields above about 1 T, terms other than the $M = 1$ term in Eq. (15) become important, and the oscillations become highly distorted. Another important feature of Eq. (15) is that for low temperature and high magnetic field the positions of the extrema in σ_{yy} will shift. At $T = 0$ K, σ_{yy} discontinuities occur at coincidence of E_F and the Landau level. At higher temperatures the extrema move to lower fields. It is also important to know that σ_{yy} does not involve the sign of the charge of the transport carrier. Thus σ_{yy} is a maximum at coincidence of E_F and a Landau level, independent of whether carriers are electrons or holes.

The Adams and Holstein theory is for a spherical Fermi surface, yet graphite has a highly distorted Fermi surface.[3] This introduces a multiplicative amplitude factor inversely proportional to the Fermi-surface curvature.[19] This does not affect the oscillation shape or magnetic field values for peaks, however.

Equation (15) assumes the Fermi energy is constant. Sugihara and Ono[18] show theoretically that the Fermi energy changes by about 10% between 2 and 4 T and by more than 20% near 6 T. It can be shown from the band-structure theory that this shift in E_F causes a shift in the fields at which Landau levels and E_F coincide. The present experiments show that the $n = 1$ electron Landau level crossing is shifted to even higher fields than predicted by Sugihara and Ono's[18] calculation. See also results presented in Ref. 16.

C. Hall Conductivity Theory

Argyres[10] calculates the Hall conductivity σ_{yx} con-

sidering only elastic scattering (ionized impurity scattering, for example) in the Born approximation. The effect of both magnetic and electric fields on the collisions is considered, and as Adams and Holstein[17] have done, he uses the density-matrix formalism. For high-symmetry directions of the magnetic field in graphite (e.g., parallel to the C axis), $\sigma_{yx} = -\sigma_{xy}$, where σ_{xy} is the Hall conductivity.[19] Under these conditions, Argyres's calculation shows that σ_{xy} has *positive* maxima at coincidence of E_F and the Landau level for *electron* carriers. For hole carriers σ_{xy} has negative extrema at coincidence of ϵ_F and the Landau level. Thus Hall-effect quantum extrema, as a function of field, depend on charge-carrier sign, while conductivity extrema do not.

Horton[22] has used the density matrix to calculate the Hall conductivity at low temperatures and high magnetic fields. Horton's results are valid for nonzero temperatures and predict the same general result as Argyres when temperatures are low: σ_{xy} has negative extrema at coincidence of E_F and the Landau level for holes.

D. Quantum Thermopower Theory

In this section we present three approaches to the theory of quantum thermopower in order to compare their applicability to experimental observations.

1. *Generalized Mott Equation*

The diffusion thermopower in the presence of a magnetic field is given by[23] the generalized Mott formula

$$\overleftrightarrow{S}(H) = \frac{\pi^2 k^2 T}{3q}\,\overleftrightarrow{\rho}(H)\cdot\left(\frac{\partial\overleftrightarrow{\sigma}(H)}{\partial E}\right)_{E_F}, \tag{16}$$

where $\overleftrightarrow{S}$, $\overleftrightarrow{\rho}$, and $\overleftrightarrow{\sigma}$ are field-dependent tensors. The factor q is positive for holes, negative for electrons, and has the magnitude of the electron charge. By definition[19,20]

$$\overleftrightarrow{S}(H) = -\overleftrightarrow{\epsilon}(H) \tag{17}$$

as given by Eq. (3). Equation (16) is a result of the linearized Boltzmann equation with elastic scattering and is therefore appropriate for ionized impurity scattering in graphite. In graphite we find experimentally

$$|\sigma_{xy}| \ll |\sigma_{yy}| \tag{18}$$

and

$$\left|\frac{\partial\sigma_{xy}}{\partial H}\right| \ll \left|\frac{\partial\sigma_{yy}}{\partial H}\right| . \tag{19}$$

From symmetry,

$$\sigma_{xz} = \sigma_{yz} = \sigma_{zx} = \sigma_{zy} = 0 ;$$

thus,

$$S_{yy}(H) \simeq \frac{\pi^2 k^2 T}{3q}\,\frac{1}{\sigma_{yy}}\left(\frac{\partial\sigma_{yy}}{\partial E}\right)_{E_F} . \tag{20}$$

From the Adams and Holstein theory[17] for σ_{yy}, we see that near coincidence of E_F with a Landau level,

$$S_{yy} \propto (\pi^2 k^2 T/3qE_F)\delta^{-1} , \tag{21}$$

where δ^{-1} has positive spikes at coincidence of E_F and a Landau level. Thus S_{yy} will have positive spikes for hole carriers ($+q$) and negative spikes for electron carriers. For $T \sim 2$ K and above, the spikes in graphite become rounded maxima. Close to 4 K in graphite we find that S_{yy} is purely sinusoidal in $1/H$.

2. *Thermodynamic Theory for S_{yy}*

To approximate the amplitude and line shape of the spike-shaped oscillations which occur at low temperature and high field, we tried an argument discussed by Callen[24] and by MacDonald.[25] They find that in a steady-state condition, and where the Joule heating is small, the Thomson heat is the specific heat of the electrons per charge, as a first approximation. This assumes a reversible process or "quasiequilibrium." It then follows that the thermopower S_{yy} is

$$S_{yy}(H) = -\frac{1}{Nq}\,\frac{\partial\Omega(H)}{\partial T} , \tag{22}$$

where N is the number of electrons and $\Omega(H)$ is the free energy of the system. Equation (22) was also derived by Obratzof[26] and others,[27,28] but they assume that $|\sigma_{xy}| \gg |\sigma_{yy}|$, a condition we did not find in graphite.

Lifshitz and Kosevich[29] have evaluated Ω for $\hbar\omega \gg kT$. Using the Lifshitz-Kosevich expression for Ω, and evaluating Eq. (22), we find

$$S_{yy} = -\frac{2k}{qn_0}\left(\frac{eH}{ch}\right)^{3/2}\left(\frac{\partial^2 A}{\partial k_z^2}\right)^{-1/2}_{(k_z)_{\max}} \times\sum_M \frac{e^{-MX_D}}{M^{3/2}}\,A_3(MX) \times\cos\left(\frac{2\pi MF}{H} - 2\pi M\gamma \mp \frac{\pi}{4}\right)\cos\frac{\pi Mgm^*}{2m_0} , \tag{23}$$

where n_0 is the density of particles, A is the extremal cross-sectional area of the Fermi surface perpendicular to the field, k_z is the component of wave vector parallel to the field, γ is a phase factor normally equal to $\frac{1}{2}$, g is a spin factor, and X_D is the "Dingle" factor which accounts for col-

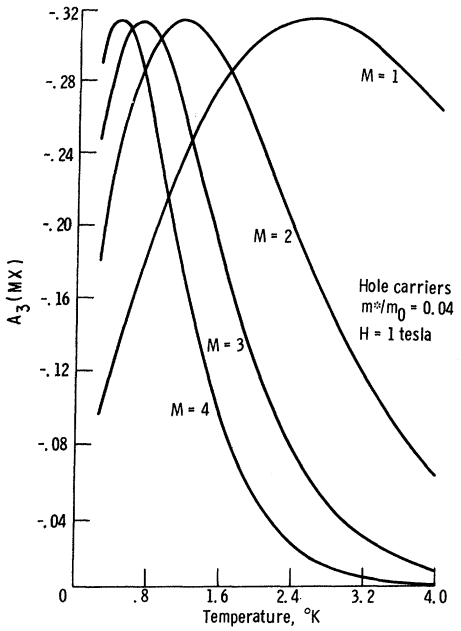

FIG. 1. $A_3(MX)$ plotted as a function of temperature [Eq. (24)] for several M values, at 1 T. The effective mass is $0.04m_0$ appropriate for holes in graphite.

lision broadening of Landau levels.[30] The term $A_3(MX)$ is given by

$$A_3(MX) = (1 - MX\coth MX)/\sinh MX\ , \qquad (24)$$

where

$$X = 2\pi^2 kT/\hbar\omega\ . \qquad (25)$$

The term A_3 is shown for graphite as a function of temperature at 1 T for $M = 1$, 2, 3, 4 in Fig. 1. From Fig. 1 and Eq. (23) it is obvious that the factor A_3 determines the amplitude and harmonic structure of the oscillations as a function of magnetic field and temperature. At low temperatures and high fields the $M = 1$ term in (23) decreases in relation to the $M = 2$, 3, etc., terms. This causes a highly distorted oscillation shape at low temperatures and high fields. A plot of Eq. (23) with parameters applicable for majority-carrier holes in graphite at 2 K is shown in Fig. 2. This figure is a plot of S_{yy} as a function of field, showing distorted oscillation shapes at high fields. Equation (23) predicts better than order of magnitude agreement with experimentally observed amplitudes. However, the shape of the distorted peaks is not correctly predicted and this result will be discussed later. It is important to present the thermodynamic, Obratzof, etc., theories because the present experiments test the applicabilities of the assumptions of these theories to graphite.

3. *Horton Thermopower Theory*

As will be discussed later, the experimentally observed distortion of oscillation peaks in thermopower is correctly predicted by a theory due to Horton.[22] Scattering is assumed to be due to random point impurities, and the calculation is for free electrons. His final expression is similar to Eq. (23) but contains a sum over both sin and cos magnetic-field-dependent terms.

Figure 3 shows S_{yy} from Horton's theory plotted at $T = 1.2$ K. The plot is for hole carriers and there are higher + spikes than − dips. A Dingle factor [Eqs. (23) and (25)] was assumed, with $T_D = 1.0$ K. As will be seen later, Fig. 3 has slightly sharper spikes than the experimental results. From a series of plots at higher and lower T_D, the T_D for our samples is estimated to be on the order of 1.5 K. Williamson[2] measured a T_D from de Haas–van Alphen effect of 1.5 ± 0.1 K for a similar sample of pyrolytic graphite. This rough agreement supports the use of a Dingle factor in Horton's expression.

Notice the highly distorted oscillation shapes in Fig. 3. For the same parameters the de Haas–van Alphen effect is not nearly as distorted. There are two reasons for the high distortions in thermopower. First, the A_3 term shown in Fig. 1 causes large "harmonic content." That is, the inclusion of many of the M terms in Horton's theory is

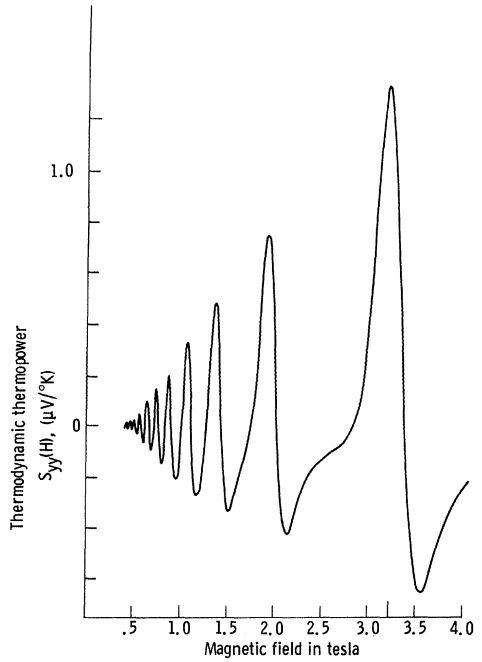

FIG. 2. Theoretical thermodynamic thermopower [Eq. (23)] plotted as a function of field at 2.0 K for hole carriers in graphite.

$$S_{xx} \propto 1.5\,H^{1/2}\sum_n \frac{(-1)^n}{n^{1/2}} A_4 \cos\left(\frac{2\pi F}{H} - \frac{\pi}{4}\right) e^{-2\pi^2 nT_D/H}$$

$$+ 79.5\,H^{1/2}\sum_n \frac{(-1)^n}{n^{1/2}} e^{-2\pi^2 nT_D/H} A_3 \sin\left(\frac{2\pi F}{H} - \frac{\pi}{4}\right)$$

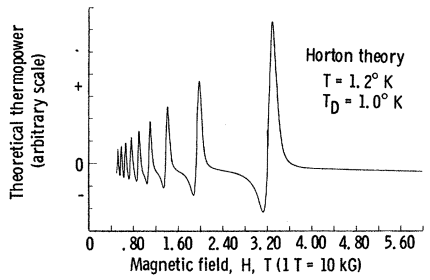

FIG. 3. Theoretical Horton thermopower plotted as a function of field at 1.2 K for hole carriers in graphite. $T_D = 1.0$ K.

necessary. The second reason is that there are two terms in his theory (see Fig. 3). At low fields the sin term is larger, but at higher fields and low temperatures the cos term causes significant distortion.

E. Energy-Band Structure of Graphite

We, as well as others, [2] have found that the properties of pyrolytic pressure-annealed graphite approach the properties of natural single crystals, and in discussing the band structure will assume the two are the same.

In McClure's notation, [31,32] the diagonal elements of the effective-mass Hamiltonian for graphite are

$$E_1 = \Delta + \gamma_1\Gamma + \tfrac{1}{2}\gamma_5\Gamma^2 ,$$
$$E_2 = \Delta - \gamma_1\Gamma + \tfrac{1}{2}\gamma_5\Gamma^2 , \qquad (26)$$
$$E_3 = \tfrac{1}{2}\gamma_2\Gamma^2 ,$$

where

$$\Gamma = 2\cos\pi\xi \qquad (27)$$

and ξ is the coordinate along k_z measured from the point K in the Brillouin zone as shown in Fig. 4. Figure 4 shows the Fermi surfaces which are located along the Brillouin-zone edges HKH. [2,3,33] Whether the charge carriers at "A" and "B" are electron or hole (one must be electron, the other hole) is associated with the signs of the band parameters. These parameters are γ_0, γ_1, γ_2, γ_3, γ_4, γ_5, Δ, and E_F, which can be determined from experiment. Magnetoreflection and de Haas–van Alphen experiments have given the best values so far [34]:

$$\gamma_0 = 2.85 \pm 0.10\ \text{eV} ,$$
$$\gamma_1 = 0.31 \pm 0.02\ \text{eV} ,$$
$$\gamma_2 = -0.0185\ \text{eV} , \leftarrow$$
$$\gamma_3 = +0.29 \pm 0.02\ \text{eV} , \qquad (28)$$
$$\gamma_4 = +0.18 \pm 0.02\ \text{eV} , \leftarrow$$
$$\gamma_5 = -0.0185\ \text{eV} , \leftarrow$$
$$\Delta = +0.009\ \text{eV} , \leftarrow$$
$$\epsilon_F = -0.022\ \text{eV} . \leftarrow$$

The signs of these coefficients were determined by Schroeder *et al.*, [8] and the constants with arrows change sign if the assignment of electrons and holes is reversed (see Fig. 4). A direct and independent determination of signs is made from the results of the present experiments as will be discussed in Sec. IV D.

In zero magnetic field the energy bands are described, neglecting γ_3, by

$$E = \tfrac{1}{2}(E_1 + E_3) \pm [\tfrac{1}{4}(E_1 - E_3)^2 + \gamma_0^2(1-\nu)^2\sigma^2]^{1/2} ,$$
$$E = \tfrac{1}{2}(E_2 + E_3) \pm [\tfrac{1}{4}(E_2 - E_3)^2 + \gamma_0^2(1+\nu)^2\sigma^2]^{1/2} , \qquad (29)$$

where E_1, E_2, and E_3 are given by Eq. (26). The normalized radial coordinate, [33] centered on the HKH edge, for directions perpendicular to k_z is given by σ, and ν is given by

$$\nu = \gamma_4\Gamma/\gamma_0 , \qquad (30)$$

where Γ is defined by Eq. (27).

In Fig. 5, energy [from Eqs. (26) and (29)] is plotted as a function of the coordinate ξ along the k_z direction for $\sigma = 0$. On the left in Fig. 5 the bands are plotted with the old signs [the negative of those indicated by arrows in Eq. (28)]. On the right in Fig. 5 the signs are those indicated in Eq. (28).

With spin-orbit interaction included in the Hamiltonian, the tips of the "A" Fermi-surface sections shown in Fig. 4 break into a separate tiny pocket

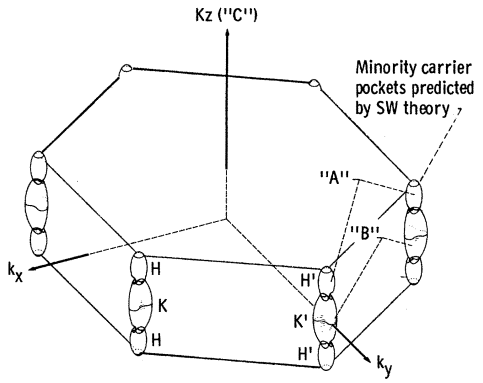

FIG. 4. Brillouin zone of graphite. The Fermi surfaces (located along H, K, H) are labeled A and B.

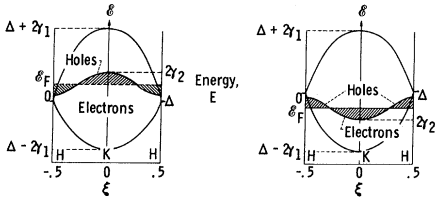

FIG. 5. Energy bands for graphite plotted against ξ, the coordinate along k_z. On the left side the old signs of band parameters are used. On the right side the new signs are used.

of carriers located at H as marked. These should give rise to very-low-frequency de Haas–van Alphen oscillations.[2,7,35]

For an existing magnetic field, the energy levels were derived by McClure[31] and Inoue[36] based on SW theory. For $\gamma_3 = 0$ the resulting secular equation is approximately

$$(n+\tfrac{1}{2})Q = \frac{E-E_3}{2}\left(\frac{E-E_1}{(1-\nu)^2}+\frac{E-E_2}{(1+\nu)^2}\right) \pm\left\{\left[\frac{E-E_3}{2}\left(\frac{E-E_1}{(1-\nu)^2}-\frac{E-E_2}{(1+\nu)^2}\right)\right]^2+\frac{Q^2}{4}\right\}^{1/2}, \tag{31}$$

where $Q = 3a_0^2\gamma_0^2 eH/2\hbar c$, and a_0 is a constant. This equation gives the energy levels as a function of magnetic field and position ξ along the edge HKH.

III. EXPERIMENTAL

Three different magnets were used for the present investigations: an 18.5-T liquid-neon-cooled "steady-state" solenoid,[37] a 10.5-T superconducting solenoid, and a 4.0-T transverse split-pair superconducting magnet. The last magnet was used when measuring thermoelectric power as a function of angle between the magnetic field and the graphite C axis. For the 10.5- and 4.0-T magnets, field measurements were accurate to within 0.2%. The samples were highly ordered pressure-annealed pyrolytic graphite. The distribution of directions of C axes of the various crystallites was measured by x-ray scattering to be on the order of less than 2°. Transmission-electron-microscope studies found typical grain size to be about 10 μ diam. The ratio of electrical resistance at 300 K to that at 4.2 K was 1.5 for sample PG 3, 9 for PG 4, and 9.5 for PG 5. By comparison, natural single crystals have had ratios ranging from 12 to 37.[3]

The sample geometry is shown in Fig. 6. For ρ_{yy} and ρ_{yx} measurements, electric current flows along the sample length ($\pm y$ direction) perpendicular to the magnetic field and voltages are recorded. The measured electric fields are $\vec{E}^*$, and

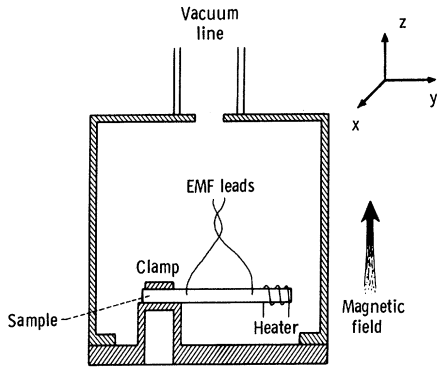

FIG. 6. Experimental geometry. The coordinate system defines components of tensors. The Z direction is defined by the magnetic field. The Y direction is defined by sample length and current flow.

from Eq. (3),

$$\vec{E}^* = \overleftrightarrow{\rho}\cdot\vec{J}, \tag{32}$$

when there are no temperature gradients. For adiabatic-thermopower ϵ'_{yy} and Nernst-Ettingshausen ϵ'_{xy} measurements, a constant heat flow $\vec{w}$ is maintained in the sample and Eq. (1) shows, when $J=0$,

$$\vec{E}^* = \overleftrightarrow{\epsilon}'\cdot\vec{w}. \tag{33}$$

To measure the thermal-resistivity-tensor components, Eq. (8) is used,

$$\vec{G} = \overleftrightarrow{\gamma}\cdot\vec{w},$$

where $\vec{G}$ is the negative-temperature-gradient vector. To calculate the tensor elements of the isothermal thermopower $\overleftrightarrow{\epsilon}$, we use Eq. (10) to obtain $\overleftrightarrow{\lambda}$ from $\overleftrightarrow{\gamma}$, and Eq. (11) to obtain $\overleftrightarrow{\epsilon}$ from $\overleftrightarrow{\epsilon}'$.

Voltages are measured with a dc nanovoltmeter and recorded against magnetic field or angle on an x-y recorder. Temperature gradients are mea-

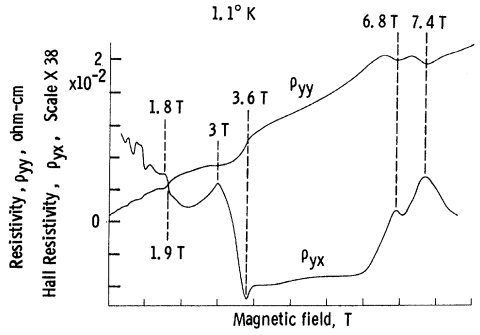

FIG. 7. Magnetoresistance ρ_{yy} and Hall resistivity ρ_{yx} plotted as a function of field at 1.1 K, for sample PG 5. ρ_{yx} has been magnified 38 times in order to show detail. 1 T = 10 kG.

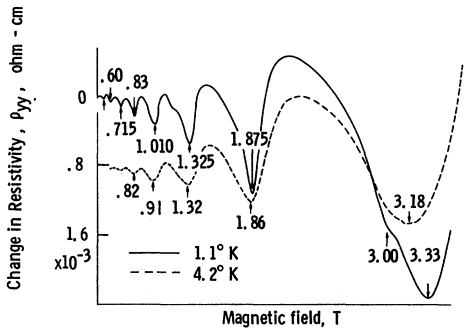

FIG. 8. Oscillatory part of magnetoresistance plotted as a function of field at 4.2 and 1.1 K. Landau level crossings of E_F marked in T.

sured with an ac wheatstone bridge. Evanohm is used for heater wire to supply the constant heat current $\vec{w}$. The power from an Evanohm heater was shown to change by less than 2% in going from 0 to 18.5 T.[38]

IV. EXPERIMENTAL RESULTS

A. Magnetoresistance

In Fig. 7 the magnetoresistance ρ_{yy} and Hall resistivity ρ_{yx} are plotted as a function of field to 10 T at 1.1 K. We find experimentally that $\rho_{yx} \ll \rho_{yy}$ and that quantum oscillations are obvious in both quantities. Using Eq. (12) for fields parallel to the high-symmetry C axis,

$$\sigma_{yy} = \rho_{yy}/(\rho_{yy}^2 + \rho_{yx}^2) \approx 1/\rho_{yy} \ . \tag{34}$$

Thus, maxima predicted by the Adams and Holstein theory[17] for σ_{yy} result in minima for ρ_{yy} when Landau levels coincide with the Fermi energy. Since $\sigma_{yy} \simeq 1/\rho_{yy}$,

$$\tilde{\rho}_{yy} \propto \tilde{\sigma}_{yy}/(\sigma_{yy}^0)^2 \ , \tag{35}$$

TABLE I. Comparison of *hole* majority-carrier extrema for Landau level crossings of E_F with predictions of Sugihara and Ono's theory (Ref. 18). The table represents data from all samples (fields in T, 1 T = 10 kG).

	Holes			
Landau level	Theoretical field position (Sugihara & Ono)	Thermopower maxima	Resistance minima	σ_{xy} minima
1	3.6	3.63 ± 0.02	3.33 ± 0.02	3.64 ± 0.1
2	1.99	1.97 ± 0.03	1.88 ± 0.02	1.94 ± 0.04
3	1.42	1.39 ± 0.02	1.33 ± 0.02	1.39 ± 0.02
4	1.10	1.08 ± 0.03	1.01 ± 0.02	1.11 ± 0.05
5	• • •	0.88 ± 0.03	0.83 ± 0.02	0.86 ± 0.03
6	• • •	0.75 ± 0.03	0.72 ± 0.03	0.75 ± 0.03
7	• • •	0.64 ± 0.03	0.60 ± 0.03	0.63 ± 0.02

TABLE II. Comparison of *electron* majority-carrier extrema for Landau level crossings of E_F with predictions of Sugihara and Ono's theory (Ref. 18). The table represents data from all samples (fields in T, 1 T = 10 kG).

	Electrons			
Landau level	Theoretical field position (Sugihara & Ono)	Thermopower minima	Resistance minima	α_{xy} maxima
1	6.4	[a]7.0: 7.68 ±0.05; 6.92 ±0.05	[a]7.2: 7.6 ±0.1; 6.8 ±0.1	[a]7.1: 7.4 ±0.1; 6.8 ±0.1
2	2.95	2.98±0.02	3.0±0.05	3.0 ±0.5
3	1.95	• • •	• • •	1.86±0.02
4	1.54	• • •	• • •	1.50±0.02
5	• • •	• • •	• • •	1.22±0.02

[a]Spin-split Landau level.

where $\tilde{\rho}_{yy}$ means the oscillatory part of the resistivity. From Eq. (15) for the oscillatory conductivity,

$$\tilde{\rho}_{yy} \propto \rho_{yy}^0 \left(\frac{\hbar\omega}{E_F}\right)^{1/2} \sum_M \frac{2\pi^2 MkT}{\hbar\omega} \sinh\left(\frac{2\pi^2 MkT}{\hbar\omega}\right)^{-1}$$
$$\times (2\pi M)^{-1/2} \cos\left(\frac{2\pi MF}{H} - \frac{\pi}{4} - \pi M\right) \ . \tag{36}$$

In Fig. 8 experimental results of the oscillatory part of the resistivity are plotted as a function of field to 4 T. At 4.2 K the oscillations are undistorted up to nearly 2 T, and the oscillations are described by the $M = 1$ term in (36) for low fields. At 1.1 K the oscillations are spike shaped and the minima shifted to higher fields. It takes more than the $M = 1$ term in (36) to describe the oscillations. In the limit of very low temperature and highly ordered crystals, the resistance minima would be very sharp and drop nearly to zero as follows from the Adams-Holstein theory.[17]

The field values for resistivity minima occurring at coincidence of E_F and Landau levels are predicted by Sugihara and Ono.[18] These are listed in Tables I and II for the quantum numbers n for the hole carriers and electron carriers, respectively. The resistivity minima from Fig. 8 for 1.1 K are also listed. As expected from the theory (Sec. II B) the resistance minima occur at slightly lower fields than Landau level crossings. Included in the table are the minima near 7 T shown in Fig. 7. At 1.1 K the weak $n = 2$ minimum due to the electron carriers is visible (Figs. 7 and 8) at 3 T. The double minima near 7 T for the $n = 1$ electron carriers is double, due to spin splitting of the Landau levels.[16] This splitting will be discussed in Sec. III E. The de Haas–van Alphen period of the minima in Fig. 8 is $0.206 \pm 0.005\ \mathrm{T}^{-1}$.

B. Hall Coefficient

Figure 9 shows a plot of resistivity ρ_{yy}, Hall resistivity ρ_{yx}, and Hall conductivity calculated from experimental ρ_{yy} and ρ_{yx} using Eq. (12). The positions of extrema in all three quantities are marked by field value and Landau quantum number. As discussed in Sec. IIC, Argyres[10] predicts that maxima will result in σ_{xy} when Landau levels for electron carriers cross E_F, and minima will result when hole levels cross E_F. In Fig. 9 $\sigma_{xy}H^2$ is plotted rather than σ_{xy} in order to best observe extrema, and has a (spin-split) maximum at 7 T, and maxima at 3.0 and 1.8 T. This series of extrema is thus due to electron carriers. Also, $\sigma_{xy}H^2$ has minima at 3.64 and 1.94 T and this series is due to hole carriers. The field values correspond to crossings of Landau levels predicted by Sugihara and Ono[18] and these are listed in Table I for holes and Table II for electrons.

By comparing the σ_{xy} extrema with resistance minima and Sugihara and Ono predictions, we find that σ_{xy} minima belong to the de Haas–van Alphen series with period $0.205 \pm 0.005\ \mathrm{T}^{-1}$. Soule, McClure, and Smith[3] have shown that this de Haas–van Alphen period belongs to the Fermi-surface section marked A in Fig. 5. This frequency assignment is also predicted by the SW band-structure theory. Thus the Fermi-surface sections at "A" in Fig. 4 are hole-type carriers.

The σ_{xy} maxima, when compared with Sugihara and Ono's predictions (Table II), are part of the de Haas–van Alphen series with period $0.16 \pm 0.01\ \mathrm{T}^{-1}$ and located at K in the Brillouin zone (Fig. 4). The Fermi-surface section B in Fig. 4 is thus the electron section. Sugihara and Ono's theory is within experimental uncertainty for all data except for the $n = 1$ (spin-split) electron level near 7 T.

C. Thermoelectric Power and Thermal Conductivity

The adiabatic coefficients are experimentally measured, but the isothermal coefficients from Eq. (1) with $J = 0$ must be calculated in order to compare with theory:

$$\vec{E}^* = \overleftrightarrow{\epsilon}' \cdot \vec{w} , \tag{37}$$

so with $\vec{w}$ in the y direction,

$$E_y = \epsilon'_{yy} w_y , \tag{38}$$

$$E_x = \epsilon'_{xy} w_y . \tag{39}$$

The coordinate convention is shown in Fig. 6. The magnetic field is maintained along the z direction. From Eqs. (38) and (39) above, a measurement of E_y with constant w_y gives ϵ'_{yy} the adiabatic thermopower, and E_x gives ϵ'_{yx} the adiabatic Nernst-Ettingshausen coefficient. To obtain the isothermal $\overleftrightarrow{\epsilon}$ tensor we use Eqs. (10) and (11). For fields along the C axis of graphite, the thermal-resistivity tensor is

$$\overleftrightarrow{\gamma} = \begin{pmatrix} \gamma_{yy} & \gamma_{xy} & 0 \\ -\gamma_{xy} & \gamma_{yy} & 0 \\ 0 & 0 & \gamma_{zz} \end{pmatrix} , \tag{40}$$

and

$$\lambda_{yy} = \gamma_{yy} / (\gamma_{yy}^2 + \gamma_{xy}^2) , \tag{41}$$

$$\lambda_{yx} = \gamma_{xy} (\gamma_{yy}^2 + \gamma_{xy}^2) . \tag{42}$$

Experimentally we find $\gamma_{xy} \ll \gamma_{yy}$ for all ranges of magnetic field; thus

$$\lambda_{yy} \simeq 1/\gamma_{yy} , \tag{43}$$

$$\lambda_{yx} \simeq \gamma_{xy}/\gamma_{yy}^2 \ll \lambda_{yy} . \tag{44}$$

The amplitude of Nernst-Ettingshausen-coefficient oscillations was found to be up to eight times larger than the thermopower. Since we found $\gamma_{yy} \geq 50\gamma_{xy}$ it follows from (10) and (11) that

$$\epsilon_{yy} \simeq \epsilon'_{yy}/\gamma_{yy} . \tag{45}$$

We have measured γ_{yy} as a function of field to 10 T and find that it "saturates" to a constant value after increasing for about 0.1–0.2 T. This saturation is due to a "freezing out" of thermal conduction by electrons. As the field increases, conductivity by electrons decreases until it is unimportant compared with lattice conduction. Lattice conduction is independent of field. We did find very weak quantum oscillations in the thermal resistivity in the saturation region of magnetic field. These were in phase with the electrical resistivity oscillations, and were attributed to electronic conductivity oscillations and *not* to phonon scattering from quantized electron states as was found for antimony.[39]

Since γ_{yy} is independent of field, Eq. (45) shows that

$$\epsilon_{yy}(H) \propto \epsilon'_{yy}(H) \tag{46}$$

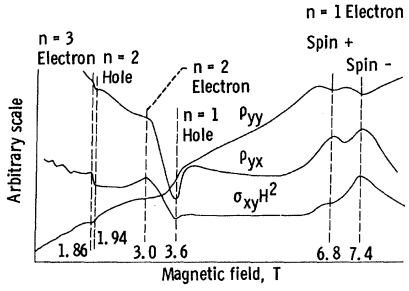

FIG. 9. Representative data for the Hall resistivity, magnetoresistance, and Hall conductivity times H^2, plotted as a function of field at 1.1 K for sample PG 5. Landau level crossings of E_F are marked in T.

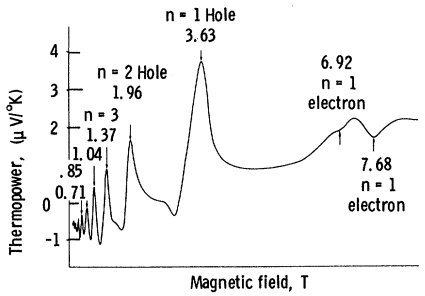

FIG. 10. Thermopower plotted against field at 1.1 K for sample PG 4. Landau level crossings for both electron (spin-split) and hole carriers are marked.

at a fixed temperature. In Ziman's[20] notation for thermopower,

$$S_{YY} = -\epsilon_{YY} . \tag{47}$$

In Fig. 10 the thermoelectric power of sample PG 4 (resistance ratio 9) is plotted as a function of field to 10 T. The field values for electron and hole extrema are marked, as well as the quantum numbers associated with each peak. In the theory (Sec. II D) it was concluded that sharp positive peaks result from hole-carrier Landau levels crossing E_F. The series 3.63 T, 1.96 T, etc., are thus due to hole Landau levels crossing E_F. They have a de Haas–van Alphen period 0.206 ± 0.007 T^{-1}. As discussed earlier, this period originates from the Fermi-surface section marked A in Fig. 4. The A surface is thus a hole surface. The minima seen in Fig. 10 at 7 T (spin split) are due to electron Landau levels crossing E_F and show that the Fermi surface B in Fig. 4 is for electrons. This assignment of electrons and holes agrees with our Hall results. We have thus provided two independent and direct experiments to confirm the assignment of electrons and holes in the Brillouin zone. This assignment agrees with the Schroeder *et al.*[8] results.

When the thermopower of sample PG 5 (resistance ratio 9.5) is plotted as a function of field, the data are the sharpest of the three samples. The same assignment of electrons and holes in the Brillouin zone results as with PG 4. An interesting part of both the PG 5 and the PG 4 data (shown in Fig. 10) is the line shape of the oscillations. The trace, as a function of increased field, rises rapidly and flattens on the high-field side. The thermodynamic theory presented in Sec. II D 2 predicts the flattening first, and the sharp drop on the high-field side as shown in Fig. 2. The same is true for the theories of Obratzof[26] and others.[27,28] However, the theory of Horton predicts the observed line shape, as shown in Fig. 3. This lends support to Horton's theory.

The observed spikes in thermopower occur at fields close to those predicted by Sugihara and Ono. The major exception is the spin-split $n = 1$ electron level centered near 7 T. This has a (spin-split) peak at a higher field than predicted. All of the observed crossings of Landau levels at E_F are listed in Tables I and II and compare favorably with Sugihara and Ono's theory.

In sample PG 3 (resistance ratio 1.5) we studied the oscillation periods ($P = 1/F$). For the electron carriers the de Haas–van Alphen period is 0.155 ± 0.005 T^{-1} for field parallel to the C axis. These oscillation periods were studied over a wide range of angle between the field and the C axis and dominated at low field and low temperature. At 4.2 K, oscillations from the *hole* Fermi surface dominated. Parallel to the C axis this period was 0.208 ± 0.008 T^{-1}. In Fig. 11 the electron and hole (majority-carrier) periods are plotted as a function of angle between the field and the C axis. The solid lines are from the natural-single-crystal data of Soule, McClure, and Smith (SMS).[3] The electron (lower-curve) period found in PG 3 was slightly higher than the SMS results, but experimental errors overlap. The period-against-angle data of Fig. 11 are characteristic of a nearly cylindrical Fermi surface, and SMS found the ratio of areas for the hole surface to be

$$A(90°)/A(0°) = 12.1 \tag{48}$$

in natural single crystals. A (0°) is the extremal cross-sectional area of the Fermi surface for field parallel to the C axis, and A (90°) is for field perpendicular to C. Within experimental error we find natural single crystals and pyrolytic graphite have identical areas for both electrons and holes out to $\pm 70°$ from C.

D. Consequences of Electron and Hole-Carrier Assignment to the Energy-Band Structure

Previous to the work of Schroeder, Dresselhaus, and Javan,[8] the energy bands were as shown on the left in Fig. 5. The parameters γ_2, γ_5, and E_F were positive, and γ_4 and Δ were negative. As shown on the right in Fig. 5, when electrons are located near the center of the zone edge ($\xi = 0$), the coefficients γ_2 and E_F reverse sign. Our quantum-Hall-effect and thermoelectric-power results confirm that holes are at A and electrons are at B, as shown in Fig. 4. This makes γ_2 and E_F negative. From (26), E_3 then has negative values. The McClure-Inoue[31,36] equation [Eq. (31)] can still be satisfied if the signs of Δ, γ_4, and γ_5 are reversed. From (26),

$$\begin{aligned} &E_1 \text{ becomes } -E_2 , \\ &E_2 \text{ becomes } -E_1 , \\ &E_3 \text{ becomes } -E_3 . \end{aligned} \tag{49}$$

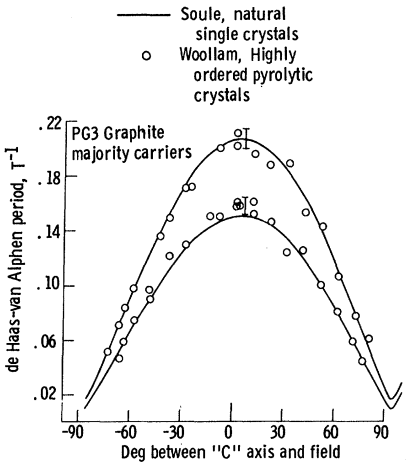

FIG. 11. de Haas–van Alphen period P plotted as a function of angle between the field and the C axis for majority carriers in sample PG 3.

In (31), replace E_1 by $-E_2$, E_2 by $-E_1$, E_3 by $-E_3$, and E by $-E$, and the equation is unchanged.

E. Spin Splitting

Spin splitting of the $n=1$ electron Landau levels is observed in the magnetoresistance (Figs. 7 and 9), the Hall coefficient (Figs. 7 and 9), and the thermopower (Fig. 10). For all of these the separation of peaks is between 0.6 and 0.7 T. This is further confirmed by the observation of very nearly the same magnitude for splitting in three different pyrolytic-graphite samples. In a natural single crystal we have recently observed splittings in the $n=1$ and $n=2$ electron levels and in the $n=1$ hole level.[16] If g is exactly 2.0, as for free electrons, then the splitting in field for the $n=1$ electron crossing at 7 T would be approximately $\Delta H \simeq 0.36$ T if all Landau level crossings of E_F were periodic in inverse magnetic field. The observed splitting in the pyrolytic samples is $\Delta H \simeq 0.6$ T and much of the increased splitting, over that corresponding to $g=2.0$, is due to the very rapid variation of the Fermi energy with magnetic field. The measured g factors and spin splittings are discussed further in another paper.[16]

V. CONCLUSIONS

The major findings of this study are the following: (a) Carriers marked A in Fig. 4 are holes and those marked B are electrons. This assignment is made from Hall effect and independently from the thermopower quantum resonances. (b) The theory of Sugihara and Ono is within experimental uncertainty of predicting the observed positions of Landau level crossings of E_F. The one exception is the $n=1$ electron level which is found higher in field than predicted. (c) Adams and Holstein's theory for the resistance of a degenerate conductor in a strong magnetic field is correct in predicting sharp maxima for σ_{yy} at the coincidence of a Landau level and the Fermi energy for both electron- and hole-type carriers. Shifts of peaks to lower fields at higher temperatures are observed. (d) A theory of Horton appears to predict the correct line shape of quantum oscillations in the thermopower at high fields. A Dingle temperature of 1.5 K gives a good fit between Horton's theory and experiment. Other theories were found not to satisfactorily explain experimentally observed wave shapes. (e) We have made the first observation of spin splitting of Landau levels in graphite. The $n=1$ electron Landau level is spin split by 0.6–0.7 T at 7 T. This provides a measure of the spin-orbit splitting at the point K in the center of the Brillouin-zone edge. (f) The thermal resistivity saturates to a constant value independent of magnetic field strength for fields above about 0.2 T. (g) Pyrolytic and natural single crystals produce the same de Haas–van Alphen frequencies as a function of angle between the field and the C axis. This lends support tc the use of the single-crystal band theory for pyrolytic samples.

ACKNOWLEDGMENTS

The author would like to thank Professor J. W. McClure for many helpful ideas and discussions. He would also like to thank Dr. D. E. Soule and Dr. G. Wagoner for helpful discussions; Dr. A. W. Moore for supplying several samples; and J. M. LaPlant and Mrs. E. A. LaSalvia for technical assistance.

[1]A. W. Moore, A. R. Ubbelohde, and D. A. Young, Proc. Roy. Soc. (London) A280, 153 (1964).
[2]S. J. Williamson, S. Foner, and M. S. Dresselhaus, Phys. Rev. 140, A1429 (1965).
[3]D. E. Soule, J. W. McClure, and L. B. Smith, Phys. Rev. 134, A453 (1964).
[4]M. S. Dresselhaus and J. G. Mavroides, Carbon 1, 263 (1964).
[5]J. C. Slonczewski and P. R. Weiss, Phys. Rev. 109, 272 (1958).
[6]J. K. Galt, W. A. Yager, and H. W. Dail, Phys. Rev. 103, 1586 (1956).
[7]D. E. Soule, IBM J. Res. Develop. 8, 268 (1964).
[8]P. R. Schroeder, M. S. Dresselhaus, and A. Javan, Phys. Rev. Letters 20, 1292 (1968).
[9]J. A. Woollam, Bull. Am. Phys. Soc. 15, 312 (1970); NASA Report No. TM X-52749 (unpublished); Phys. Letters 32A, 115 (1970).
[10]P. N. Argyres, Phys. Rev. 117, 315 (1960).
[11]J. D. Cooper, J. Woore, and D. A. Young, Nature 225, 721 (1970).
[12]V. V. Kechin, Fiz. Tverd. Tela 11, 1788 (1969)

[Soviet Phys. Solid State 11, 1448 (1970)].
[13]I. L. Spain, J. Chem. Phys. 52, 2763 (1970).
[14]J. W. McClure, in Proceedings of the Conference on the Physics of Semimetals and Narrow Gap Semiconductors, Dallas, Texas, 1970 (unpublished); J. Phys. Chem. Solids (to be published).
[15]G. Wagoner, Phys. Rev. 118, 647 (1960).
[16]J. A. Woollam, Phys. Rev. Letters 25, 810 (1970).
[17]E. N. Adams and T. D. Holstein, J. Phys. Chem. Solids 10, 254 (1959).
[18]K. Sugihara and S. Ono, J. Phys. Soc. Japan 21, 631 (1966).
[19]J. A. Woollam, Phys. Rev. 185, 995 (1969), and references therein.
[20]J. M. Ziman, *Electrons and Phonons* (Oxford U. P., Oxford, England, 1962).
[21]J. W. McClure and W. J. Spry, Phys. Rev. 165, 809 (1968).
[22]P. B. Horton, Ph. D. thesis, Louisiana State University, 1964 (unpublished).
[23]G. Fair and P. Taylor, Bull. Am. Phys. Soc. 15, 1252 (1970); and H. J. Trodahl (unpublished).
[24]H. G. Callen, Phys. Rev. 73, 1349 (1948).
[25]D. K. C. MacDonald, *Thermoelectricity* (Wiley, New York, 1962), p. 11.
[26]Y. N. Obraztsov, Fiz. Tverd. Tela 7, 455 (1965) [Soviet Phys. Solid State 7, 573 (1965)].
[27]P. S. Zyrganov and Kalashnikov, Fiz. Metal. i Metalloved. 18, 166 (1964).
[28]K. D. Tsêndin and A. L. Éfros, Fiz. Tverd. Tela 8, 306 (1966) [Soviet Phys. Solid State 8, 378 (1966)].
[29]I. M. Lifshitz and A. M. Kosevich, Zh. Eksperim. i Teor. Fiz. 29, 730 (1956) [Soviet Phys. JETP 2, 636 (1956)].
[30]R. B. Dingle, Proc. Roy. Soc. (London) A211, 517 (1952).
[31]J. W. McClure, Phys. Rev. 119, 606 (1960).
[32]J. W. McClure, Phys. Rev. 108, 612 (1957).
[33]J. W. McClure, IBM J. Res. Develop. 8, 255 (1964).
[34]P. R. Schroeder, M. S. Dresselhaus, and A. Javan, in Conference on the Physics of Semimetals and Narrow Gap Semiconductors, Dallas, Texas, 1970 (unpublished); J. Phys. Chem. Solids (to be published).
[35]J. A. Woollam (unpublished).
[36]M. Inoue, J. Phys. Soc. Japan 17, 808 (1962).
[37]J. C. Laurence, NASA Report No. TN D-4910, 1968 (unpublished).
[38]J. A. Woollam, Rev. Sci. Instr. 41, 284 (1970).
[39]J. R. Long, C. G. Grenier, and J. M. Reynolds, Phys. Rev. 140, A187 (1965).

PHYSICAL REVIEW B VOLUME 3, NUMBER 4 15 FEBRUARY 1971

Polarization Effects in the Electroreflectance of Bismuth Telluride at Oblique Incidence*

A. Balzarotti
Istituto di Fisica dell'Università di Roma, Roma, Italy

and

E. Burattini and P. Picozzi
Istituto di Fisica dell'Università dell'Aquila, Aquila, Italy

(Received 3 August 1970)

The optical transitions above the threshold of the uniaxial crystal bismuth telluride have been investigated by means of electroreflectance over the energy range 1–5.5 eV using an electrolyte to produce electric fields at the surface. Both near-normal and oblique incidence measurements were made using light polarized under different orientations of the electric vector with respect to the *c* axis. The combination of these techniques permitted an unambiguous identification of the symmetry of the critical points and yielded the precise polarization dependence of the transitions. The broad electroreflectance spectra of bismuth telluride have been understood and analyzed in terms of strongly lifetime-broadened Franz-Keldysh tunneling. A correlation, although preliminary, has been attempted with the band structure of this material.

I. INTRODUCTION

Recent theoretical and experimental papers have raised new interest in the optical properties of bismuth telluride and of other rhombohedral crystals of the homologous group, bismuth selenide and antimony telluride.

Besides the early work of Lee and Pincherle,[1] based upon an augmented-plane-wave (APW) calculation of the band structure of bismuth telluride, two more theoretical works appeared which made use of the pseudopotential approach. Borghese and Donato[2] have evaluated the band structure of bismuth telluride at the high-symmetry points of the Brillouin zone including the spin-orbit interaction, and have tried to interpret the reflectivity spectra of Greenaway and Harbeke[3] and to check the galvanomagnetic data of various authors. Their results agree with the six-valley model for both conduction and valence bands,[4–7] but their interpretation of the high-energy optical transitions differs remarkably from that given by Greenaway and Harbeke.

More recently Katsuki[8] calculated the band energy also along lower-symmetry lines and on the reflec-